Chinese Journal of Catalysis 68 (2025) 230–245

available at www.sciencedirect.com

ScienceDirect

journal homepage: www.sciencedirect.com/journal/chinese-journal-of-catalysis

Article

# Dimethoxymethane carbonylation and disproportionation over extra-large pore zeolite ZEO-1: Reaction network and mechanism

Shaolei Gao [a,b], Peng Lu [c], Liang Qi [a,*], Yingli Wang [a], Hua Li [a], Mao Ye [a], Valentin Valtchev [d], Alexis T. Bell [e,f], Zhongmin Liu [a,b,*]

[a] *National Engineering Research Center of Lower-Carbon Catalysis Technology, Dalian National Laboratory for Clean Energy, Dalian Institute of Chemical Physics, Chinese Academy of Sciences, Dalian 116023, Liaoning, China*

[b] *University of Chinese Academy of Sciences, Chinese Academy of Sciences, Beijing 100049, China*

[c] *The ZeoMat Group, Qingdao Institute of Bioenergy and Bioprocess Technology, Chinese Academy of Sciences, Qingdao 266101, Shandong, China*

[d] *Université de Caen Normandie, ENSICAEN, CNRS, LCS, Caen 14000, France*

[e] *Lawrence Berkeley National Laboratory, Berkeley, California 94720, United States*

[f] *Department of Chemical and Biomolecular Engineering, University of California, Berkeley, California 94720, United States*

ARTICLE INFO

*Article history:*
Received 23 October 2024
Accepted 25 November 2024
Available online 10 January 2025

*Keywords:*
Dimethoxymethane carbonylation
Dimethoxymethane disproportionation
Zeolite
*In-situ* IR
Kinetic
Reaction mechanism

ABSTRACT

Methyl methoxyacetate (MMAc) and methyl formate (MF) can be produced directly by heterogeneous zeolite-catalyzed carbonylation and disproportionation of dimethoxymethane (DMM), with near 100% selectivity for each process. Despite continuous research efforts, the insight into the reaction mechanism and kinetics theory are still in their nascent stage. In this study, ZEO-1 material, a zeolite with up to now the largest cages comprising 16×16-MRs, 16×12-MRs, and 12×12-MRs, was explored for DMM carbonylation and disproportionation reactions. The rate of MMAc formation based on accessible Brönsted acid sites is 2.5 times higher for ZEO-1 (Si/Al = 21) relative to the previously investigated FAU (Si/Al = 15), indicating the positive effect of spatial separation of active sites in ZEO-1 on catalytic activity. A higher MF formation rate is also observed over ZEO-1 with lower activation energy (79.94 *vs.* 95.19 kJ/mol) compared with FAU (Si/Al = 30). Two types of active sites are proposed within ZEO-1 zeolite: **Site 1** located in large cages formed by 16×16-MRs and 16×12-MRs, which is active predominantly for MMAc formation, and **Site 2** located in smaller cages for methyl formate/dimethyl ether formation. Kinetics investigation of DMM carbonylation over ZEO-1 exhibit a first-order dependence on CO partial pressure and a slightly inverse-order dependence on DMM partial pressure. The DMM disproportionation is nearly first-order dependence on DMM partial pressure, while it reveals a strongly inverse dependence with increasing CO partial pressure. Furthermore, ZEO-1 exhibits good catalytic stability, and almost no deactivation is observed during the more than 70 h test with high carbonylation selectivity of above 89%, due to the well-enhanced diffusion property demonstrated by intelligent-gravimetric analysis.

© 2025, Dalian Institute of Chemical Physics, Chinese Academy of Sciences.
Published by Elsevier B.V. All rights reserved.

## 1. Introduction

Production of carbonyl-containing chemicals is usually limited by the utilization of noble metal complexes. Hence, an

* Corresponding author. E-mail: qlyanfei920@dicp.ac.cn (L, Qi) , zml@dicp.ac.cn (Z, Liu).

This work was supported by the National Natural Science Foundation of China (22472173), the Youth Innovation Promotion Association, the Chinese Academy of Sciences (2023193), the starting grant provided by Qingdao Institute of Bioenergy and Bioprocess Technology, the Shandong Energy Institute (SEI S202107) and the Qingdao Institute of Bioenergy and Bioprocess Technology International Collaboration Project (202305).
https://doi.org/10.1016/S1872-2067(24)60187-7

economic, efficient, non-metal based heterogenous catalytic route for the production of carbonyl-containing chemicals is highly desired. Methyl methoxyacetate (MMAc) and methyl formate (MF), two of the most important carbonyl-containing chemicals, can be produced directly by zeolite-catalyzed carbonylation and disproportionation of dimethoxymethane (DMM), using a heterogeneous catalyst, and with near 100% selectivity for each process [1–3].

MMAc obtained by carbonylation of DMM can serve as a precursor for producing monoethylene glycol (MEG), glycolic acid (GA), and methyl glycolate (MG) via routes **A** and **B** shown in Fig. 1 [1–7]. In route **A**, MMAc is hydrogenated to 2-methoxyethanol and then hydrated to produce MEG, an important commodity chemical with a global demand of over 28 million metric tons per year. Currently, MEG is produced by epoxidation of ethylene, sourced by dehydrogenation of ethane derived from shale gas or as a by-product of petroleum processing, and subsequent liquid-phase, thermal hydration of the resulting ethylene oxide (EO) using a large excess of water ($H_2O$/EO = 20–25) [8]. MEG can also be produced by hydrogenation of dimethyl oxalate (DMO) obtained by carbonylation of $CH_3ONO$ over $PdCl_2$ in the presence of $Cl_2$, a corrosive and explosion-prone process [9]. Route **B** illustrates the direct hydration of MMAc to produce GA and MG, monomers for biodegradable polymers. The production of GA has previously been explored by liquid-phase carbonylation of formaldehyde using strong acids and high carbon monoxide pressures (tens to hundreds of atmospheres) [10].

In the absence of CO addition to DMM, the only reaction is DMM disproportionation, which produces MF and dimethyl ether (DME) (route **C** in Fig. 1). MF is one of the most important intermediates in C1 chemistry that is widely used for the production of more than 50 chemicals and has a global output of more than 6 million tons in 2016 [11]. Industrial MF production it is still limited to methanol carbonylation using homogeneous catalysts that exhibit low efficiency. The employed catalyst is sodium methoxide, a strong base, which is sensitive to water, resulting in process operating difficulties [12].

Zeolite-catalyzed DMM conversion provides an efficient heterogenous routes for producing MF, MEG and GA. A pilot-test plant for GA production based on zeolite-catalyzed DMM carbonylation, developed by the Dalian Institute of Chemical Physics, was completed successfully in 2022 [13]. Since DMM is formed via the reaction of methanol with formaldehyde (a product of methanol oxidation) and methanol is produced from synthesis gas, DMM conversion also offers a novel, syngas-based route for the production of various oxygen-containing chemicals. Moreover, if syngas is produced by steam reforming/gasification of biomass or hydrogenation of $CO_2$ captured from atmosphere, one can envision the sustainable production of all products shown in Fig. 1.

As first reported by Bell and co-workers, the carbonylation and disproportionation of DMM can be promoted by zeolites [1–3]. The elementary steps involved in these processes are envisioned to occur *via* reactions R1–R6 shown below. Both carbonylation and disproportionation are initiated by the reaction of DMM with a Brönsted acid proton to form methoxymethyl (MMZ) species. MMZ carbonylation forms a new C–C bond between the C atom of CO and the terminal methylene C atoms of MMZ to generate methoxy acyl (MAZ) species. MAZ then undergoes methoxylation *via* reaction with DMM to generate MMAc. Besides, the attack of MMZ by DMM leads to the generation of adsorbed formyl (MFZ) groups and, finally, to the formation of MF and DME via DMM disproportionation.

$$\text{Z-H + DMM} \rightarrow \text{Z-CH}_2\text{OCH}_3 + \text{CH}_3\text{OH} \quad \text{(R1)}$$

$$\text{Z-CH}_2\text{OCH}_3\text{+ DMM} \rightarrow \text{Z-CH}_3\text{OCHOCH}_3 + \text{DME} \quad \text{(R2)}$$

$$\text{Z-CH}_3\text{OCHOCH}_3 \rightarrow \text{Z-COH + DME} \quad \text{(R3)}$$

$$\text{Z-COH + DMM} \rightarrow \text{Z-CH}_2\text{OCH}_3 + \text{MF} \quad \text{(R4)}$$

$$\text{Z-CH}_2\text{OCH}_3 + \text{CO} \rightarrow \text{Z-COCH}_2\text{OCH}_3 \quad \text{(R5)}$$

$$\text{Z-COCH}_2\text{OCH}_3 + \text{DMM} \rightarrow \text{Z-CH}_2\text{OCH}_3 + \text{MMAc} \quad \text{(R6)}$$

Celik *et al.* [1,2] have reported that the activity and selectivity for DMM carbonylation and disproportionation are sensitive to the size of the zeolite cages and channels and to the Si/Al ratio. Examination of FAU, MOR, BEA, and MFI showed that FAU was the most effective catalyst for DMM carbonylation to MMAc because of its high rate of MMAc formation and low rate of DMM disproportionation. The high selectivity of FAU (~70%) was attributed to its large supercage, which disfavor disproportionation. The effects of zeolite confinement in MFI vs FAU have also been investigated theoretically by Shapovalov

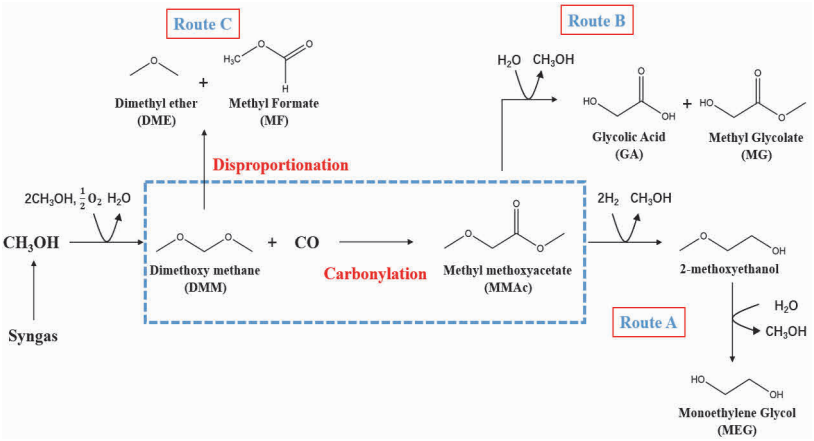


**Fig. 1.** The DMM conversion pathways for the production of MEG, GA, MG, and MF from syngas. DMM carbonylation process for new C–C bond formation is outlined in blue.

and Bell [4]. This work showed that while the activation barriers of MMZ carbonylation to MAZ over MFI and FAU zeolites were comparable, the activation barrier for methoxylation of MAZ by DMM relative to the barrier for MAZ decomposition was significantly lower for FAU than that for MFI. Energy decomposition analysis revealed that this effect of zeolite structure was due to more significant electronic stabilization of the transition state for MAZ in FAU than in MFI [4]. Relative to FAU, the smaller pores of MFI, MOR, and BEA force the reactants into an orientation that promotes the hydrogen transfer process, the critical step of DMM disproportionation. On the other hand, BEA zeolite with 12 × 12 MRs intersection was found to favor disproportionation much more effectively than MFI in the temperature range of 360–420 K [1], which might be due to the higher diffusivity of DMM in 12-MRs channels.

The zeolite Si/Al ratio also affects the rate of MMAc formation over FAU, BEA, and MFI [1]. As reported, low Al density zeolites led to higher carbonylation rates because with fewer Al atoms within the zeolite framework, Al centers and the species adsorbed on them are spaced farther apart, thereby avoiding repulsive electrostatic interactions between these species. The closer proximity of surface species in high Al density zeolites is envisioned to increase the activation energy in the cationic transition state for nucleophilic attack during the process of DMM carbonylation and disproportionation.

The prior studies of zeolite-catalyzed DMM carbonylation and disproportionation demonstrate that the structure of zeolite plays a critical role in determining the catalytic activity and selectivity to MMAc and MF. However, a fundamental understanding of the structure-performance relationship for these processes remains unclear. Specifically, it is not known whether the FAU supercage is optimally favorable for DMM carbonylation. Investigation of the DMM disproportionation is rarely performed. In recent years, a new type of extra-large-pore zeolites, i.e., the ZEO family, has been developed, which provides the possibility to explore the effects of larger reaction space for DMM carbonylation [14–16]. A prominent member of this new family of zeolites is ZEO-1, an extra-large pore zeolite containing Brönsted acid sites [14]. ZEO-1 has a 3D channel system comprised of 16-MRs and 12-MRs channels that generate cages formed by 16×16-MRs, 16×12-MRs, and 12×12-MRs [14]. These cages have four windows of 16-MRs and/or 12-MRs, with those involving 16-MRs being larger than the 12-MRs windows in the supercage of FAU. The application of ZEO-1 zeolites in new reaction processes for large-size carbonyl-containing chemicals [17] certainly deserves particular attention.

Here, we report a systematic investigation of both DMM carbonylation and disproportionation over ZEO-1 zeolite and compare its activity and product selectivity with those of FAU-type zeolite. Since the channels formed by 16-MRs are larger than that of most zeolites [18–20], they decrease the intracrystalline barrier for diffusion of DMM and its products. We show in this study that the rate of MMAc formation per accessible protons over ZEO-1 is 2.5 times higher than that for FAU with slightly lower Si/Al ratio of ~15. ZEO-1 also exhibits excellent stability during a 70 h DMM carbonylation test. It is also notable that while the kinetics of MMAc formation over ZEO-1 and FAU are comparable, the kinetics of DMM disproportionation differ. For FAU, the reported rate of MF/DME formation is independent of CO partial pressure, whereas for ZEO-1, the rate first decreases and then levels off with increasing CO partial pressure. This behavior is similar to that observed for MFI, and suggests the presence of sites located in the small cages of ZEO-1 that are more active for DMM disproportionation. Within these cages, MMZ rapidly converts to MAZ when CO is present, leading to a decrease in the rates of MF and DME formation. This interpretation is supported by *in-situ* IR observations. This study offers new directions for catalytic utilization of large-pore zeolites.

## 2. Experimental

### 2.1. Materials and reagents

ZEO-1 (IZA code: JZO) zeolite with a Si/Al ratio of ca. 21 was synthesized referred to a previously reported two-step process [14]. The first step is the synthesis of the organic structure directing agent (OSDA), tricyclohexylmethylphosphonium hydroxide (TCyMPOH), which is achieved by mixing tricyclophosphine (Aladin, 98%) with excess methyl iodide (Energy Chemical, 99.5%) in acetonitrile and subsequent reaction at room temperature for two days. Subsequently, the solvent was evaporated to obtain the powder iodide salt. The iodide form of the OSDA was converted to its hydroxide form via ion exchange in batch mode using anion exchange resin (Xidian, 1.1 milliequivalent per milliliter). The hydroxide solution was concentrated by rotary evaporation under vacuum. The concentration of the final solution was determined by titration with 0.1 mol $L^{-1}$ HCl (Beijing North Weiye Institute of Measuring and Testing Technology) using phenolphthalein as an indicator.

The second step was the synthesis of ZEO-1 zeolite using a gel with molar composition of $1.0SiO_2$:$0.02Al_2O_3$:$0.5TCyMP(OH)_2$:$10H_2O$. Aluminum isopropoxide (Macklin, AR) was dissolved in TCyMPOH solution in a plastic beaker under magnetic stirring, followed by slow addition of tetraethyl orthosilicate (TEOS, Sinopharm, ≥99%). The mixture was kept stirring to obtain a clear sol, which was then hydrolyzed at ambient temperature overnight to remove water and ethanol formed by hydrolysis. The sol was then heated at 373 K in a convection oven to remove residual water and ethanol to reach the target gel molar composition by weighting. The viscous gel was transferred into a Teflon-lined autoclave and heated at 463 K in a convection oven statically for 30 d. The solid product was recovered by centrifugation and washing three times with water (200 mL), ethanol (100 mL) and acetone (100 mL). The resulting cake was dried at 373 K for 12 h, and then calcined at 873 K for 12 h. The phosphorous species left in the calcined zeolite was removed by washing with hot water and then dried at 373 K and calcined at 873 K for 3 h.

FAU (Si/Al = 15 and 30) zeolites were purchased from Zeolyst. CO (99.99%) was purchased from Dalian Special Gas Corporation and dimethoxymethane (DMM, 98%) was purchased from Shanghai Aladdin Biochemical Technology Co., Ltd. All reagents were used without any extra treatments.

### 2.2. Catalyst characterization

Powder X-ray diffraction (XRD) patterns of the as-synthesized samples were recorded by a PANalytical X'Pert PRO X-ray diffractometer using Cu $K_\alpha$ radiation ($\lambda$ = 0.154059 Å) at 40 kV and 40 mA from 3° to 36°. Si/Al ratio of as-synthesized ZEO-1 zeolite was determined by PerkinElmer 7300DV inductively coupled plasma optical emission spectrometer (ICP-OES). $N_2$ adsorption and desorption analysis was carried out on a Micromeritics ASAP 2020 analyzer. About 0.2 g ZEO-1 was evacuated at 623 K for 4 h before recording. The total surface area was calculated based on the Brunauer-Emmett-Teller (BET) method. The micropore volume and area were determined by the t-plot method. $^{27}$Al NMR spectra were collected on Bruker Avance III 400 MHz spectrometer. TEM images were performed on JEM-2100 Transmission Electron Microscope.

Infrared (IR) spectra of adsorbed pyridine were recorded on a Bruker VERTEX 70 instrument equipped with a mercury cadmium telluride (MCT) detector. The samples (about 15 mg) were pressed into a self-supporting wafer and placed into an *in-situ* cell. The samples were pretreated at 573 K for 1 h under $N_2$ before recording. The samples were recorded in the range of 4000 to 1000 cm$^{-1}$ after cooling down to 423 K. Then, pyridine was introduced and IR spectra were acquired by averaging 64 scans with a resolution of 4 cm$^{-1}$ at 423 K after desorbing pyridine at corresponding temperature for 30 min.

*In-situ* IR spectra characterizing DMM carbonylation and disproportionation were recorded on Bruker VERTEX 70V with a mercury cadmium telluride (MCT) detector. The samples (about 15 mg) were pressed into a self-supporting wafer and placed into a metal *in-situ* cell. The samples were pretreated at 723 k for 30 min under Ar. Meanwhile *in-situ* IR system was evacuated to remove atmosphere water vapor and $CO_2$ before recording. The samples were recorded in the range of 4000 to 1000 cm$^{-1}$ by averaging 64 scans with a resolution of 4 cm$^{-1}$ every 30 s continuously after cooled down to reaction temperature (383 K) and increased to the reaction pressure (0.4–0.5 MPa) with the introduction of reaction gases.

The uptake rates of *n*-pentane in ZEO-1 and FAU (Si/Al = 30) zeolite were measured on an IGA-100 intelligent gravimetric analyzer (IGA). About 20–30 mg samples were first degassed at 623 K for 2 h to a constant weight. The gaseous *n*-pentane was then introduced to the cell and the adsorption kinetics curve was recorded at 293–313 K and 3 mbar.

### 2.3. Catalytic testing

DMM carbonylation and disproportionation were carried out in a fixed-bed reactor. A K-type thermocouple was used to measure the reaction temperature and a back pressure valve was placed in the outlet of the reactor. The reactor is made of stainless steels with a quartz lining of 8 mm inner diameter. 6.5–100 mg catalysts were loaded in the middle of the quartz lining supported on quartz wool. Dimethoxymethane (DMM) was sealed into a stainless autoclave with an inlet fitted under the liquid surface and an outlet above the liquid surface. The stainless autoclave was placed in a water bath system to keep DMM at a fixed temperature. Before reaction, the catalyst was pretreated with 50 mL min$^{-1}$ $N_2$ at 773 K for 1 h. Then, DMM mixed with CO was introduced into the reactor at 363–463 K, space velocity = 18–923 L $g_{cat}^{-1}$ h$^{-1}$ at 1-5 MPa to test DMM carbonylation and DMM mixed with $N_2$ was introduced into the reactor at 343–423 K, space velocity = 36–108 L $g_{cat}^{-1}$ h$^{-1}$ at 1 MPa to evaluate DMM disproportionation. The products were analyzed online by a gas chromatograph (Agilent 7890B) equipped with a HP-PLOT-Q capillary column and a flame ionization detector (FID).

DMM conversion and products selectivity (Eq. (2) for DMM carbonylation and Eqs. (3), (4) for DMM disproportionation) were determined by Eqs. (1)–(4). $C_x$ indicates molar concentration of product *x*, *x* can be MMAc, MF and DME.

$$C_{DMM} = (C_{DMM,in} - C_{DMM,out})/C_{DMM,in} \quad (1)$$

$$S_{MMAc} = 3C_{MMAc}/(2C_{DME} + 2C_{MF} + C_{MeOH} + 3C_{MMAc}) \quad (2)$$

$$S_{MF} = 2C_{MF}/(2C_{DME} + 2C_{MF} + C_{MeOH}) \quad (3)$$

$$S_{DME} = 2C_{DME}/(2C_{DME} + 2C_{MF} + C_{MeOH}) \quad (4)$$

## 3. Results and discussion

### 3.1. Physical and chemical properties of ZEO-1

Crystal structure and physical properties of ZEO-1 zeolite were investigated. The X-ray powder diffraction (XRD) pattern of ZEO-1 zeolite shown in Fig. 2(a) displays a typical diffraction pattern of JZO topology [14], with no other diffraction peaks observed, indicating the high purity of ZEO-1. The $N_2$ adsorption-desorption isotherm (Fig. 2(b)) is type-IV with a steep step in the 0.80 < $p/p_0$ < 0.99 region, which demonstrated the presence of textural mesopores. Analysis of this isotherm gives a mesopore volume of 0.90 cm$^3$ g$^{-1}$, which is much higher than most of FAU [21,22]. Further analysis of the isotherm shows that the micropore and mesopore surface areas for ZEO-1 are 518 and 328 m$^2$ g$^{-1}$, respectively. Transmission electron microscopy (TEM) images (Figs. 2(c), (d)) show that the crystal size of as-synthesized ZEO-1 is about 20–40 nm. The Si/Al ratio of ZEO-1 as determined by ICP-OES is 21, whereas that of the commercial FAU samples used in this study is 15 and 30, re-

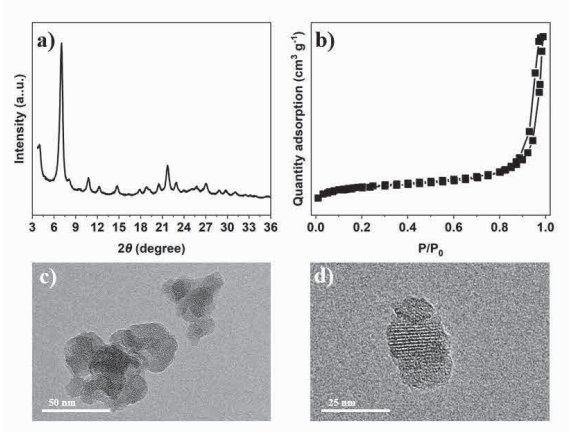


**Fig. 2.** Crystal structure and physical properties of ZEO-1 zeolite. XRD pattern (a), $N_2$ adsorption-desorption isotherms (b), and low and high-resolution TEM images (c,d) of ZEO-1 zeolite.

spectively. $^{27}$Al MAS NMR (Fig. S1) reveals that about 69% of the total Al for ZEO-1 is framework Al and 31% is extra-framework Al, consistent with earlier observation [14]. Infrared (IR) spectra following pyridine adsorption were conducted to characterize the acidity of ZEO-1 and FAU zeolite, and the results are presented in Fig. S2.

### 3.2. DMM disproportionation over ZEO-1

DMM disproportionation to MF/DME was firstly investigated without CO co-feeding. Figs. 3(a) and (b) show the influence of temperature on the rate of DMM disproportionation over ZEO-1 zeolite. As the reaction temperature increases from 343 to 423 K for a constant feed composition and flowrate, the DMM conversion remarkably increases from 16.1% to 99.3%, and the molar ratio of DME to MF in products remains close to 2:1, in accord with the mechanism for DMM disproportionation proposed previously [1,2]. Over this temperature range, the rate of MF formation per Brönsted acid site (i.e., the turnover frequency (TOF)) increases from 19.2 to 111.7 $h^{-1}$ (mol $mol_{Brönsted\ acid\ site}^{-1}$ $h^{-1}$). The influence of space velocity was also investigated. As the space velocity increased from 36 to 108 $L^{-1}$ $g_{cat}^{-1}$ $h^{-1}$, at 373 K and for an inlet DMM partial pressure of 17 kPa, the DMM conversion decreased from 83.8% to 64.7%, and the TOF for MF formation increased from 64.5 to 149.8 $h^{-1}$, as depicted in Figs. 3(c) and (d), suggesting the high activity of ZEO-1 zeolite for DMM disproportionation.

The influence of DMM partial pressure was investigated at 373 K (Figs. 3(e) and (f)). As DMM partial pressure increased from 10 to 27 kPa, the DMM conversion decreased only from 72.3% to 61.3%, but the MF formation rate increased almost linearly from 33.5 to 74.8 $h^{-1}$. As mentioned earlier, the formation of MMZ, the precursor for DMM disproportionation, is facile. The near first-order dependence of the rates of MF formation on DMM partial pressure indicates that the surface concentration of MMZ remains near saturation until the end of the reactor, where the DMM partial pressure falls for conditions leading to high DMM conversion. Furthermore, it can be deduced that the rate-limiting step is the reaction of DMM with MMZ, consistent with what has been proposed in studies conducted with FAU [2].

DMM conversion is nearly 100% and MF formation rate reaches 111.7 $h^{-1}$ at 423 K, as shown in Fig. 3(c). Therefore, a high DMM disproportionation activity over ZEO-1 is proved. Initial literature reports indicated that relatively small reaction space, like BEA and MFI, could catalyze DMM disproportionation much more effectively [2,3], which might be contributed by the enhanced H-transfer process between two DMM molecular. ZEO-1 contains 12×12 MRs cages, whose size is comparable with BEA, and could exhibit high DMM disproportionation

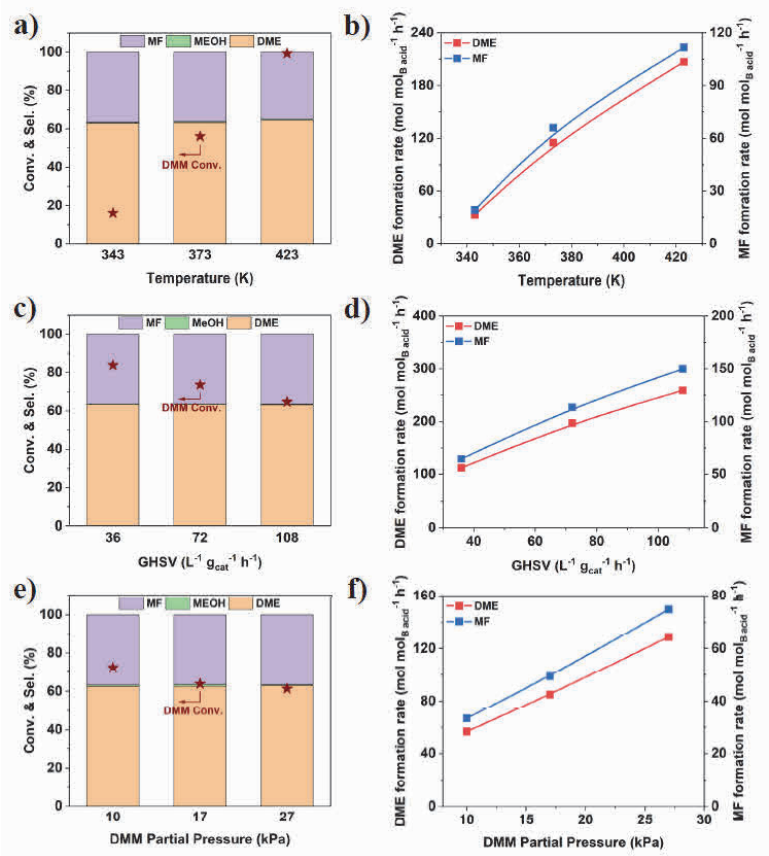


**Fig. 3.** DMM disproportionation over ZEO-1 as a function of reaction temperature (a,b), space velocity (c,d), and DMM partial pressure (e,f). Reaction conditions: (a,b): 0.05 g ZEO-1, 343–423 K, $P_{DMM}$ = 27 kPa, space velocity = 36 L $g_{cat}^{-1}$ $h^{-1}$ at total pressure of 1 MPa (balanced with $N_2$); (c,d): 0.05 g ZEO-1, 373 K, $P_{DMM}$= 17 kPa, space velocity = 36-108 L $g_{cat}^{-1}$ $h^{-1}$ at total pressure of 1 MPa (balanced with $N_2$); (e,f): 0.05 g ZEO-1, 373 K, $P_{DMM}$= 10–27 kPa, space velocity = 36 L $g_{cat}^{-1}$ $h^{-1}$ at total pressure of 1 MPa (balanced with $N_2$).

activity.

### 3.3. DMM carbonylation over ZEO-1

DMM carbonylation was investigated over ZEO-1 for temperatures between 383 and 443 K at a total pressure of 3 MPa, of which the DMM partial pressure was 43 kPa and the CO partial pressure was 2.96 MPa, and the total gas flowrate was 30 mL $min^{-1}$ (Figs. 4(a) and (b)). At 383 K, ZEO-1 exhibits similar MMAc selectivity compared to that of FAU (Si/Al = 30) (ca. 83.6% *vs.* 84.8%) and a comparable DMM conversion (60.3% *vs.* 59.1%) (Fig. S3). As the reaction temperature increases under conditions of constant pressure and feed composition, the TOF for MMAc formation over ZEO-1 increases slightly to a maximum value of 116.1 $h^{-1}$ at 393 K and then decreases monotonically as the temperature increases further to 443 K. Over this temperature range, the MMAc selectivity decreases monotonically from 83.6% to 46.8%, and is accompanied by increased formation rate of MF and DME. These data indicate that high MMAc selectivity and formation rate are achieved at ca. 393 K. The decrease of MMAc formation rate with the increase of temperature (> 400 K) could be attributed to two factors: one is the competitive reaction of DMM disproportionation, of which activity increases monotonically with the increase of temperature; the other is the decomposition of MMAc, the carbonylation product, through a reverse process as shown in Fig. S6.

The effects of total pressure on DMM carbonylation over ZEO-1 at 383 K are presented in Figs. 4(c) and (d). For these experiments, the molar ratio of DMM to CO in the feed was maintained at 1:69. The TOF for MMAc formation increases from 66.8 to 97.8 $h^{-1}$, and MMAc selectivity increases from 61.9% to 83.6%, as the pressure increases from 1 to 3 MPa. High conversion of DMM of around 60.3% is observed over ZEO-1 zeolite at total pressure of 3 MPa, and that over FAU (Si/Al = 30) is similar, TOF for MMAc and MMAc selectivity increasing from 36.7 to 60.0 $h^{-1}$ and 75.2% to 84.6%, respectively, as pressure increased from 1 to 3 MPa (Fig. S4). Increasing total pressure diminishes the rate of DMM disproportionation relative to the rate of MMAc formation, leading to an increase in MMAc selectivity.

Figs. 4(e) and (f) show DMM conversion, product selectivity as well as the formation rates of MMAc and MF, measured at 383 K and 43.2 kPa DMM at a total pressure of 3 MPa over ZEO-1 zeolite, as a function of the space velocity. As can be seen, the rate of MMAc formation increases almost linearly with increasing space velocity initially but then increases further at a much lower rate for higher space velocity. Notably, no discernible trend is evident in the MMAc selectivity with increasing space velocity, indicating that DMM carbonylation and disproportionation are parallel reactions. The influence of space velocity for FAU (Si/Al = 30) is quite similar to that for

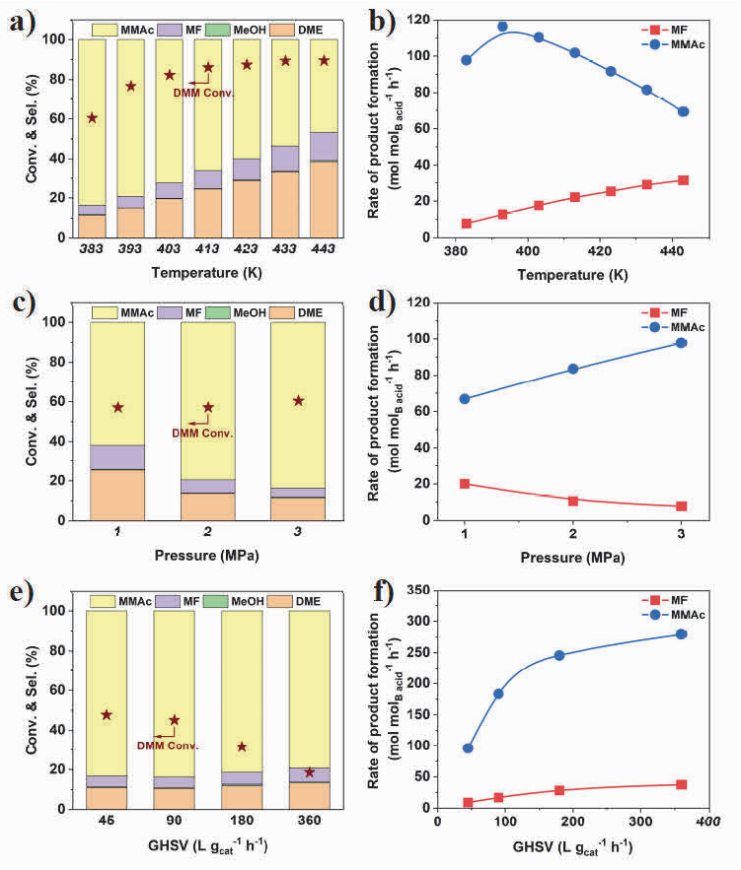


**Fig. 4.** DMM carbonylation and disproportionation over ZEO-1 as a function of reaction temperature (a,b), total pressure (c,d) and space velocity (e,f). Reaction conditions: (a,b) 0.05 g zeolite, 373–443 K, $P_{DMM}$ = 43 kPa, space velocity = 36 L $g_{cat}^{-1}$ $h^{-1}$ at 3 MPa; (c,d) 0.05 g zeolite, 383 K, $P_{DMM}$ = 14.3–43 kPa, space velocity = 36 L $g_{cat}^{-1}$ $h^{-1}$ at 1-3 MPa; (e,f) 0.02 g zeolite, 383 K, $P_{DMM}$ = 43 kPa, space velocity = 45–360 L $g_{cat}^{-1}$ $h^{-1}$ at 3 MPa.

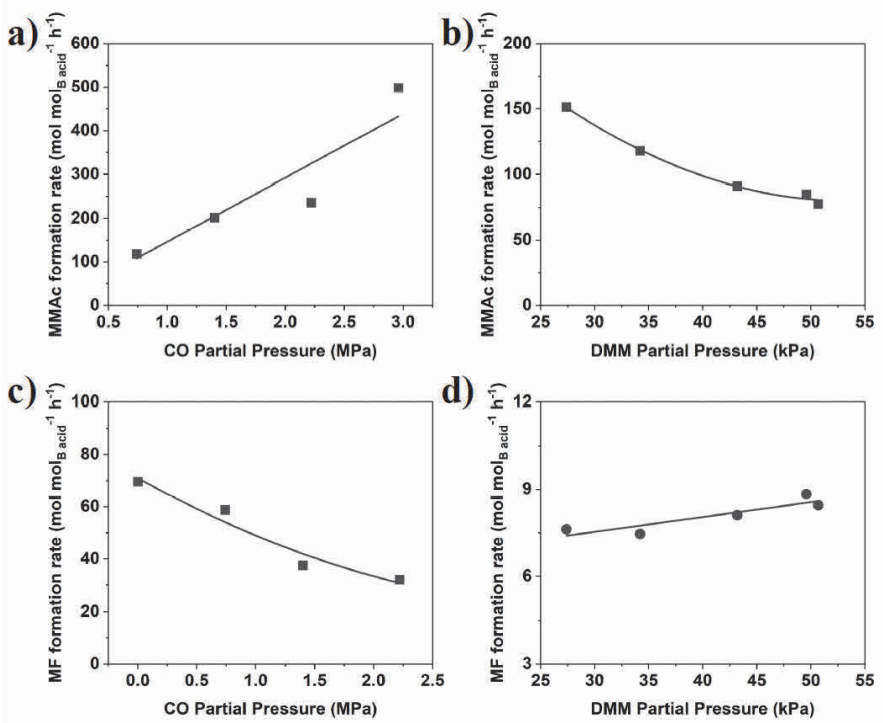


**Fig. 5.** Dependence of the rates of DMM carbonylation to MMAc and disproportionation to MF over ZEO-1 measured at 353–373 K, on the CO partial pressure (a,c) and DMM partial pressure (b,d). Reaction conditions: (a,c) 0.0065 g ZEO-1, 373 K, $P_{DMM}$ = 43 kPa, $P_{CO}$ = 0.74–2.96 MPa at total pressure of 3 MPa, (b,d) 0.0113 g ZEO-1, 353 K, $P_{DMM}$ = 27–52 kPa at total pressure of 3 MPa.

ZEO-1 (Fig. S5).

Therefore, both ZEO-1 and FAU exhibit good DMM carbonylation activity and selectivity and we attribute them to the comparable large voids of 16×16 MRs and 16×12 MRs cages in ZEO-1 and supercage in FAU. In large void, DMM disproportionation to DME and MF is suppressed since the nucleophilic attack from CO to generate methoxy acyl is kinetically more favorable. Moreover, since the methoxylation of methoxy acyl is facile in large void, high DMM carbonylation activity and selectivity is then achieved over both ZEO-1 and FAU.

The dependence of the rates of DMM carbonylation and disproportionation on the partial pressures of CO and DMM are presented in Fig. 5. These data were acquired for DMM conversions of < 15%. The rate of MMAc formation exhibits a linear dependence on CO partial pressure (Fig. 5(a)), similar to that reported for FAU [6]. MF formation rate both shows positive dependence on DMM partial pressure for ZEO-1 and FAU. However, the rate of MF formation rate displays a strong negative dependence on CO partial pressure (Fig. 5(b)), in contrast to what has been reported for FAU, which shows an almost zero-order dependence (0–0.3 MPa) [2].

The similarity and difference of DMM conversion over ZEO-1 and FAU may indicate the kinetically different catalytic behavior for carbonylation and disproportionation over these two zeolites. A wider distribution of zeolite cages containing 16×16-MRs, 16×12-MRs, and 12×12-MRs in ZEO-1 demonstrates that DMM carbonylation and disproportionation could occur over Brönsted acid sites within different reaction spaces. As mentioned in the introduction part, the reaction space could influence the formation and the transformation of reaction intermediates, especially for MAZ. Moreover, it is anticipated that the site occupancy will change with the evolving surface intermediate, thereby altering the competitive reaction rates and selectivity. More detailed analysis will be discussed in Mechanism and Kinetics Analysis section.

To assess the intrinsic carbonylation activity, the TOF normalized by accessible Brönsted acid sites for MMAc formation over ZEO-1 and FAU was performed at 373 K with a CO/DMM feed ratio of 45.5 and total pressure of 2 MPa, under near differential reaction conditions. In the case of ZEO-1 and FAU, the

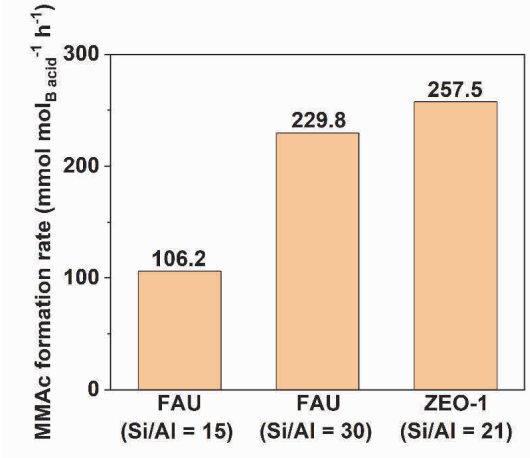


**Fig. 6.** Comparison of DMM carbonylation activity over ZEO-1 and FAU under low conversion. For ZEO-1: 0.01 g ZEO-1, 373 K, $P_{DMM}$ = 43 kPa, GHSV = 360 L $g_{cat}^{-1}$ h$^{-1}$ at 2 MPa. For FAU (Si/Al = 15): 0.05 g FAU, 373 K $P_{DMM}$ = 43 kPa, GHSV = 240 L $g_{cat}^{-1}$ h$^{-1}$ at 2 MPa. For FAU (Si/Al = 30): 0.02 g FAU, 373 K, $P_{DMM}$ = 43 kPa, GHSV = 600 L $g_{cat}^{-1}$ h$^{-1}$ at 2 MPa.

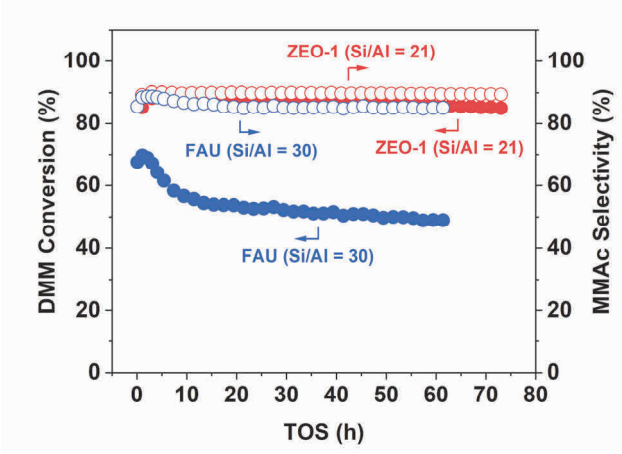


**Fig. 7.** DMM carbonylation over ZEO-1 and FAU (Si/Al = 30). Reaction conditions: 0.1 g zeolite, 383 K, $P_{DMM}$ = 14 kPa, space velocity = 18 L $g_{cat}^{-1}$ $h^{-1}$ at 5 MPa.

DMM conversion was < 15%. As shown in Fig. 6, the TOF of MMAc formation over ZEO-1 is 257.5 $h^{-1}$, 2.5 times higher than that for FAU (Si/Al = 15). Additionally, based on the preceding discussion, the Si/Al ratio of FAU zeolite affects the spatial distance, and proximal Al species would generate repulsive electrostatic interactions between adsorbed surface species. Therefore, FAU zeolite with a higher Si/Al ratio of 30 was also applied for comparison. As observed, FAU (Si/Al = 30) zeolite exhibited higher TOF activity than its counterpart with a lower Si/Al ratio of 15, but comparable to that for ZEO-1 with Si/Al ratio of 21 (229.8 *vs.* 257.5 $h^{-1}$). The higher TOF for FAU (Si/Al = 30) relative to FAU (Si/Al = 15) is ascribed to the larger distance between Al atoms in the FAU (Si/Al = 30), which reduces the repulsive forces between neighboring MMZ species [1]. What is notable, though, is the TOF for MMAc formation over ZEO-1 (Si/Al = 21) and FAU (Si/Al = 30) are nearly the same. Therefore, it appears that the larger spacing between zeolite framework Al atoms in an extra-large-pore zeolites, i.e., ZEO-1, offers sufficient room to avoid repulsive electrostatic interactions between surface species and realize the efficient carbonylation of DMM.

Long time on-stream tests were performed to compare the activity and stability of ZEO-1 and FAU (Si/Al = 30) for MMAc formation, as seen in Fig. 7. Under the reaction conditions evaluated, the conversion of DMM decreased from 69.7% to 48.9% for FAU (Si/Al = 30) after about 65 h of time on stream. By contrast, for ZEO-1, the DMM conversion decreased slowly from 88.5% to 85.0% over more than 70 h of time on stream. The MMAc selectivity remained above 89.0% for ZEO-1, while the MMAc selectivity decreased gradually from 89% to 85% for FAU (Si/Al = 30). Therefore, it is evident that ZEO-1 and FAU exhibit virtually comparable MMAc selectivity; However, ZEO-1 is more active and significantly more stable than FAU. The well-enhanced catalytic stability for ZEO-1 can be ascribed to faster diffusion through this zeolite. The size of 16-MRs diffusion channel of ZEO-1 is 9.45 Å, larger than that of FAU (7.29 Å), as reported by Chen *et al.* [14]. Further comparison of the zeolite diffusion property was performed by the uptake rates of *n*-pentane over ZEO-1 and FAU zeolite through an intelligent gravimetric analyzer (IGA). *n*-pentane was selected because its size is close to that of DMM. ZEO-1 demonstrated comparable adsorption velocity of *n*-pentane molecular at 293 K (Fig. S7) but faster at higher temperature (303–313 K for Figs. S8 and S9) compared with FAU (Si/Al = 30), proving that diffusion through ZEO-1 is superior to that through FAU, especially at higher temperature.

### 3.4. Reaction mechanism investigated by in-situ IR spectroscopy

*In-situ* IR spectroscopy was used to probe the adsorption of DMM as well as the generation of intermediates and products during DMM carbonylation and disproportionation. Possible pathways for the formation of adsorbed species involved in

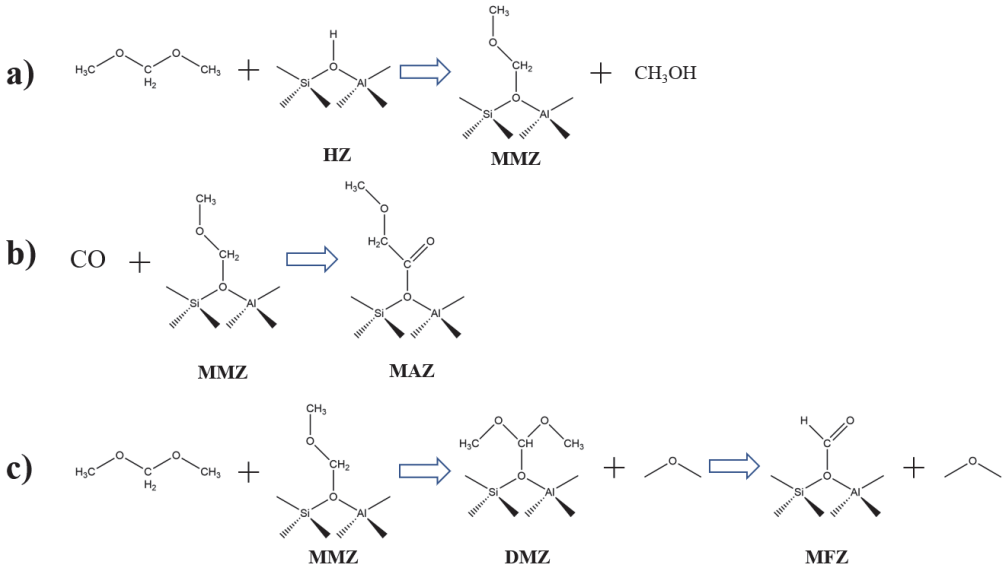


**Fig. 8.** Schematic illustration for the formation of MMZ *via* the interaction of DMM with Brönsted acid sites over zeolite (a), MAZ via CO insertion into MMZ (b), and MFZ *via* a hydrogen transfer reaction between DMM and MMZ (c).

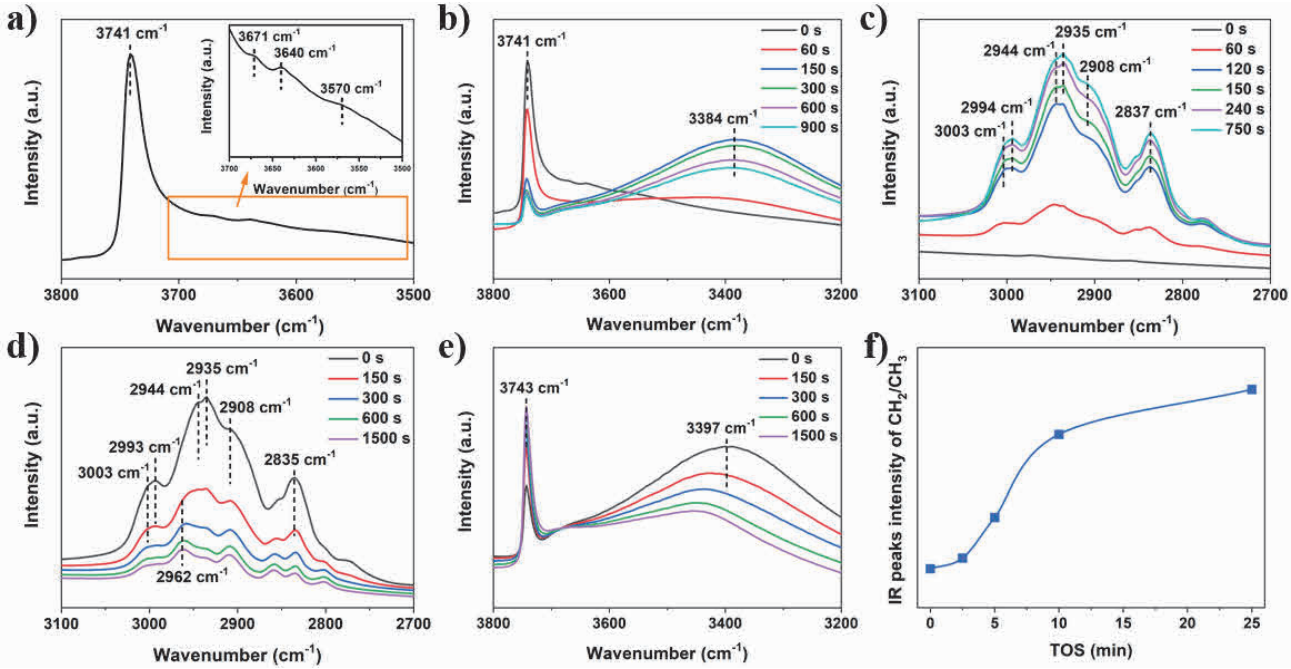


**Fig. 9.** (a) IR spectrum of surface hydroxyl groups on ZEO-1. *In-situ* IR spectra of ZEO-1 exposed to 8 kPa DMM/Ar (b,c) and Ar purge after DMM/Ar (d,e). (f) Plots of the IR intensity representing $CH_2/CH_3$ versus purging time. Conditions: 0.015 g ZEO-1, 383 K, 100 mL $min^{-1}$ total flow rate at a total pressure of 0.4 MPa.

these two processes are illustrated in Fig. 8. The stable structures formed are designated as MMZ, MAZ, DMZ, and MFZ, respectively.

IR spectra acquired during the exposure of ZEO-1 to a flow of DMM in Ar are shown in Fig. 9. Prior to the introduction of DMM into the IR cell, four peaks were observed at 3741, 3671, 3640 and 3570 $cm^{-1}$ in the O–H stretching part of the spectrum (Fig. 9(a)). The peak at 3741 $cm^{-1}$ is attributable to hydroxyl groups associated with isolated silanol groups, whereas the peaks at 3671, 3640, and 3570 $cm^{-1}$ are hydroxyl groups associated with extra-framework Al species, bridging hydroxyl groups that exhibits Brönsted acid property and a band which could be internal silanol groups or bridging hydroxyl groups or a mixture of both, respectively [23–26]. Upon introduction of the DMM/Ar mixture, the hydroxyl groups were consumed, and a broad peak appeared centered at 3384 $cm^{-1}$, the intensity of which increases initially but then slightly decreases (Fig. 9(b)). This peak is attributed to hydrogen-bonded DMM [2,27]. Purging the cell with Ar following the introduction of the DMM/Ar mixture resulted in partial recovery of the intensity of the peak at 3743 $cm^{-1}$ and that at 3397 $cm^{-1}$ corresponding to hydrogen-bonded DMM (Fig. 9(d)). While the intensity of bridging hydroxyl groups representing zeolite protons remained constant during the purging process. These observations indicate that DMM H-bonded with silanol groups is reversible and not as strong as those adsorbed at Brönsted acid sites.

Furthermore, upon introduction of the DMM/Ar mixture, Figs. 9(c) and 9(e) show that peaks appearing at 3003 and 2837 $cm^{-1}$ attributable to asymmetric and symmetric stretching vibrations of $–CH_3$ groups, and at 2944 and 2908 $cm^{-1}$ attributable to asymmetric and symmetric $–CH_2$ stretching vibrations, respectively [2,28]. The IR band at 2935 $cm^{-1}$ represents the stretching vibration of $–CH_3$ group. The intensity of the band at 2944 $cm^{-1}$ for $\nu_a(–CH_2)$ increases more slowly than the intensity at 2935 $cm^{-1}$ for $\nu_s(–CH_3)$, suggesting the gradual generation of MMZ [2]. Purging the IR cell with Ar after 750 s of exposure to the DMM/Ar mixture results in the gradual removal of adsorbed DMM, together with any MF and DME produced by DMM disproportionation, as evidenced by the gradual decrease in peak intensities in the region of 3100–2700 $cm^{-1}$ (Fig. 9(e)). After removal of gaseous and physically adsorbed DMM, DME, and MF, peaks associated with $–CH_3$ stretching vibrations should decrease to a greater degree than those associated with $–CH_2$ stretching vibration since the molar ratio of $–CH_2$ to $–CH_3$ is one in MMZ and 0.5 in DMM. Figs. 9(e) and (f) show that the ratio of the intensity of the peak at 2944 $cm^{-1}$ (shifted to 2962 $cm^{-1}$ gradually with Ar purge, for asymmetric stretching of C-H of $–CH_2$ groups) to the peak at 2935 $cm^{-1}$ (principally due to symmetric C–H stretches of $–CH_3$ groups) increases gradually, consistent with the formation of MMZ [2]. The evolution of these IR signals during DMM introduction and removal demonstrates the interaction of DMM with Brönsted-acidic protons and the generation of surface MMZ groups, a critical intermediate during DMM conversion.

DMM disproportionation is the only process that occurs when DMM interacts with ZEO-1. This process leads to the generation of MFZ, the precursor to MF (Fig. 8(c)). Formation of both MFZ and MF is evidenced by the appearance of bands for carbonyl stretching vibrations in the region of 1700 to 1800 $cm^{-1}$, as seen in Fig. 10(a). The assignment and comparison for peak intensity of these C=O stretching vibrations for ZEO-1 and FAU is summarized in Table 1. For ZEO-1, peaks at 1766, 1753 and 1733 $cm^{-1}$ were observed after introducing the DMM/Ar mixture (Fig. 10(a)). The peaks at 1766 and 1753 $cm^{-1}$ are due

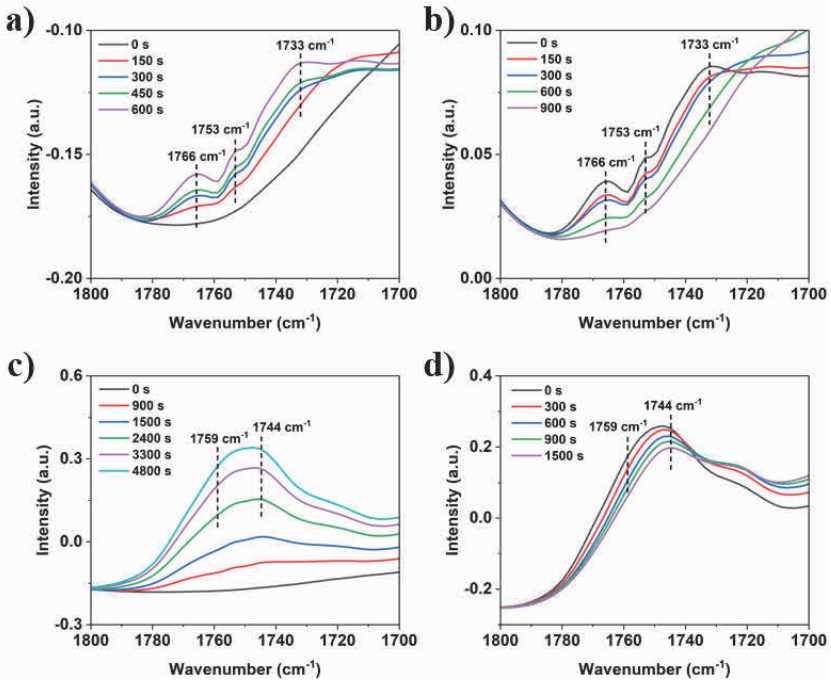


**Fig. 10.** *In-situ* IR spectra of ZEO-1 collected during exposed to 8 kPa DMM/Ar (a), Ar purging after DMM/Ar (b), exposed to 8 kPa DMM/CO (c) and Ar purging after DMM/CO (d). Conditions: 0.0157 g ZEO-1 for (a,b) and 0.0140 g ZEO-1 for (c,d), 383 K, 100 mL $min^{-1}$ total flow rate at total pressure of 0.5 MPa.

to the R branch and Q branch of gaseous MF and the band at 1733 $cm^{-1}$ is ascribed to MFZ [2,29,30]. Similar IR spectra acquired with FAU exhibit peaks at 1766, 1753, and 1736 $cm^{-1}$ (Fig. 11(a)). The relative peak intensities of these peaks are similar for both zeolites, with the peak at 1733 or 1736 $cm^{-1}$ exhibiting the highest intensity (Figs. 10(a) and 11(a)). The intensity of the peak at 1733 $cm^{-1}$ is higher for ZEO-1 than that for FAU, consistent with the higher rate of DMM disproportionation over ZEO-1 versus FAU (Fig. 4 and Figs. S3–S5). All peaks attributed to DMM disproportionation disappeared after Ar purge for 900 s, as shown in Fig. 10(b), indicating the weak adsorption and fast diffusion of DMM disproportionation related species, DME, MF and MFZ in ZEO-1 zeolite.

IR spectra acquired during DMM carbonylation over ZEO-1 with DMM/CO co-feeding were shown in Figs. 10(c) and (d). Compared with DMM disproportionation, CO-feeding leads to two new IR bands at around 1744 and 1759 $cm^{-1}$, ascribed to the C=O stretching vibration of MAZ and MMAc (Fig. S11), respectively. After exposure of the zeolite to the DMM/CO mixture for initial 900 s, the peak in 1733 $cm^{-1}$, attributed to MFZ could hardly be observed, indicating DMM disproportionation is highly inhibited. With extended reaction time, the intensity of the peaks at 1744 and 1759 $cm^{-1}$ both increased gradually (Fig. 10(c)). Ar purge after DMM carbonylation was shown in Fig. 10(d). After Ar purge for 1500 s, most of peaks related to MMAc and possible DMM disproportionation species disappeared and only MAZ could be observed at 1744 $cm^{-1}$.

IR spectra for DMM carbonylation were obtained over FAU as well. After introducing the DMM/CO mixture, two C=O stretching vibration peaks of MAZ and MMAc were observed at

**Table 1**
The assignment and area of IR peaks for FAU (Si/Al = 30) and ZEO-1 with identical feed compositions.

| Wavenumber ($cm^{-1}$) | Assignment | (Area/$\mu mol_{Brönsted\ acid}$) | | | |
|---|---|---|---|---|---|
| | | FAU [f] | ZEO-1 [f] | FAU [g] | ZEO-1 [g] |
| 1766 [a] | MF | 0.137 | 0.158 | — | — |
| 1759 [b] | MMAc | — | — | 8.06 | 3.30 |
| 1753 [c] | MF | 0.0263 | 0.0216 | — | — |
| 1744 [d] | MAZ | — | — | 10.29 | 8.21 |
| 1733/1736 [e] | MFZ | 0.388 | 0.711 | — | — |

[a] 1766 $cm^{-1}$ assigned to R branch of gaseous MF.
[b] 1759 $cm^{-1}$ assigned to C=O stretching vibration of MMAc.
[c] 1753 $cm^{-1}$ assigned to Q branch of gaseous MF.
[d] 1744 $cm^{-1}$ assigned to C=O stretching vibration of MAZ.
[e] 1733 and 1736 $cm^{-1}$ assigned for MFZ over ZEO-1 and FAU, respectively.
[f] 383 K, $P_{DMM}$ = 8 kPa, 100 mL $min^{-1}$ total flow rate of DMM/Ar at total pressure of 0.5 MPa and normalized by Brönsted acid density.
[g] 383 K, $P_{DMM}$ = 8 kPa, 100 mL $min^{-1}$ total flow rate of DMM/CO at a total pressure of 0.5 MPa and normalized by Brönsted acid density.

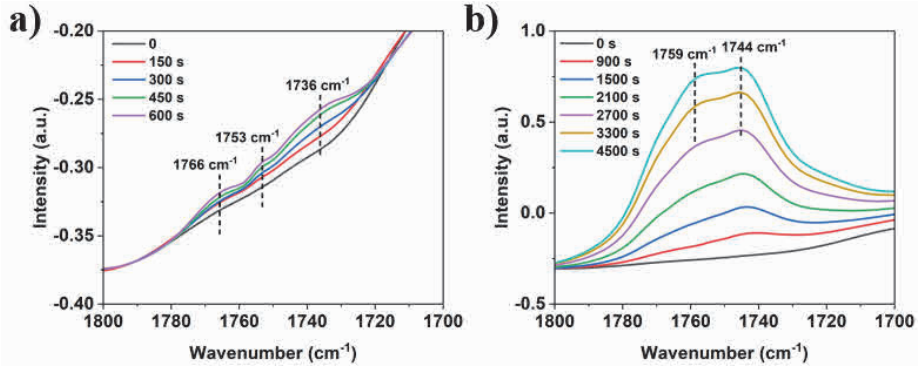


**Fig. 11.** *In-situ* IR spectra of FAU (Si/Al = 30) collected during exposed to 8 kPa DMM/Ar (a) and 8 kPa DMM/CO (b), respectively. Conditions: 0.0115 g FAU for (a) and 0.0134 g FAU for (b), 383 K, 100 mL min$^{-1}$ total flow rate at total pressure of 0.5 MPa.

1744 and 1759 cm$^{-1}$ (Fig. 11(b)). With the increase of reaction time, the peak of MMAc at 1759 cm$^{-1}$ increased slower at first but then faster than that of MAZ at 1744 cm$^{-1}$, in accord with the initial accumulation of DMM carbonylation intermediate, MAZ, and the latter formation of DMM carbonylation product, MMAc (Figs. 10(c) and 11(b)).

To further confirm the attribution of the IR peak positions for MFZ and MAZ involving C=O group, an IR spectrum was acquired during catalyst exposure to $^{13}$CO and DMM. ZEO-1 was used because it exhibits an intense band at 1744 cm$^{-1}$. As seen in Fig. 12, the introduction of $^{13}$CO/DMM mixture to ZEO-1 results in a spectroscopic evolution like that observed when DMM/Ar is fed (Fig. 10(a)). Notably, the peaks for C=O vibrations between 1720 and 1780 cm$^{-1}$, again show bands at 1766, 1753, and 1733 cm$^{-1}$ related to DMM disproportionation, with the ratios of peak intensities similar to that observed in Fig. 10(a). However, the peak at 1744 cm$^{-1}$ observed when $^{12}$CO/DMM is fed (Fig. 10(c)) is replaced by a peak at 1703 cm$^{-1}$ (Figs. 12 and S12). Since the carbonyl in MAZ stems from CO insertion, the ~40 cm$^{-1}$ bathochromic shift of the carbonyl band in MAZ upon switching from $^{12}$CO to $^{13}$CO is consistent with expectation [31]. By contrast, the chemical processes shown in Figs. 10, 12 and S12 indicate that the carbonyl C atom

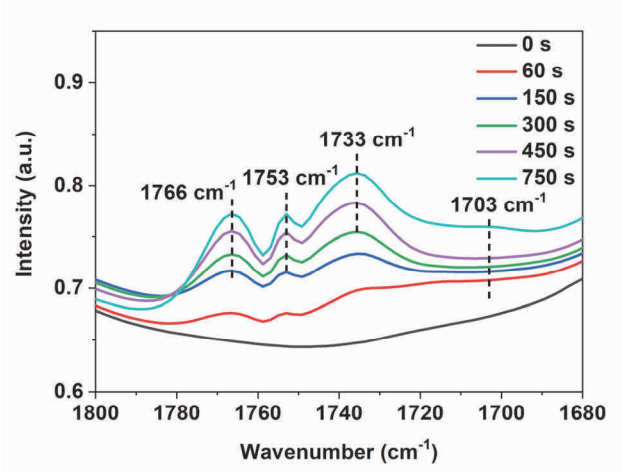


**Fig. 12.** *In-situ* IR spectrum of ZEO-1 collected during exposed to 8 kPa DMM/$^{13}$CO. Conditions: 0.015 g ZEO-1, 383 K, 25 mL min$^{-1}$ total flow rate at total pressure of 0.1 MPa.

in MF and MFZ originates from DMM, and hence, the position of the IR peaks for MFZ and MF for these species remains unchanged.

For zeolite-catalyzed DMM carbonylation, it has been proposed that the formation of acyl species is the rate-limiting step unless the methoxylation step for ester formation is sterically inhibited, as has been observed for DMM carbonylation over MFI zeolite [4,32,33]. The conversion of acyl cations through nucleophilic attack has been reported to be facile in zeolites with large internal voids [34,35]. For the conversion of methoxyacetyl cations with DMM in FAU, the activation energy has been reported to be 16 kJ mol$^{-1}$. For comparison, the activation energy is in the range of 6.6–10.7 kJ mol$^{-1}$ for the reaction of an acetyl cation with furan in BEA zeolite [34,35]. Considering that most of the cages in ZEO-1 are larger than or comparable to those in FAU, the methoxylation activation barrier of MAZ could be similar or lower. Therefore, MAZ formation *via* CO insertion to adsorbed MMZ species is proposed to be the rate-limiting step in DMM carbonylation over ZEO-1.

With the clear identification of IR bands ascribed to intermediates formed during DMM conversion, the difference in DMM carbonylation activity between ZEO-1 and FAU is expected to correlate qualitatively with the surface concentration of MAZ, as reflected by the area of the peak at 1744 cm$^{-1}$. Table 1 shows that the peak area of the MAZ signal at 1744 cm$^{-1}$ for ZEO-1 is comparable with that for FAU (Si/Al = 30) (8.21 *vs.* 10.29 area/μmol$_{\text{Brönsted acid}}$), consistent with the similar carbonylation activity of ZEO-1 and FAU (Si/Al = 30). Since ZEO-1 contains larger 16-MRs channels, the much lower peak area of 1759 cm$^{-1}$ for MMAc adsorbed in ZEO-1 (3.30 *vs.* 8.06 area/μmol$_{\text{Brönsted acid}}$) could be ascribed to its more rapid diffusion at higher temperature than what occurs in FAU (Figs. S7–S9). For DMM disproportionation, the intensity of the IR peak for MFZ at 1736 or 1733 cm$^{-1}$ is also ca. 2 times higher for ZEO-1 than that for FAU (0.711 *vs.* 0.388 area/μmol$_{\text{Brönsted acid}}$), consistent with the higher rate of DMM disproportionation over ZEO-1 versus FAU. The similarity in the ratio of peak intensities characterizing MAZ (comparable) and MFZ (2 times higher) suggests the similarity in the relative rates of DMM carbonylation and disproportionation over the two zeolites, as seen in Figs. 4 and S3–S5.

### 3.5. Mechanism and kinetics analysis

Based on our experimental results and the mechanism for DMM conversion over FAU proposed in the literature, we propose the mechanism for ZEO-1 catalyzed DMM carbonylation and disproportionation shown in Fig. 13 [2]. DFT calculations have confirmed that ZEO-1 contains 21 kinds of T sites in either 12-MRs or 16-MRs channels. T11 in 12-MRs is the most probable aluminum location, while T7 in 16-MRs is the nest preferable aluminum location [26]. The selectivity of DMM carbonylation to MMAc over BEA, ZEO-1 and FAU was performed under identical reaction conditions (Fig. S13). ZEO-1 exhibits an MMAc selectivity of 83.7%, which lies between that of BEA (63.1%) and FAU (84.8%). Al located in 16-MRs channels of ZEO-1 shares larger or comparable space to the supercage in FAU [14] and exhibits a higher MMAc selectivity than that of FAU. Moreover, for the Al located in 12-MRs channels of ZEO-1, the distance between adjacent Al is larger or comparable to that of BEA [14], and exhibits a higher MMAc selectivity than that of BEA. Therefore, the intermediate MMAc selectivity of ZEO-1 suggests that Al atoms located at both types of channels, differing in relative activity and/or selectivity for each reaction. Two categories of active sites could be divided as followed, large cages associated with 16×16-MRs and 16×12-MRs intersection, referred to as **Site 1**, and small cages associated with 12×12-MRs intersection, referred to as **Site 2**. We propose that DMM carbonylation to form MMAc occurs preferentially on **Site 1**, whereas DMM disproportionation occurs preferentially on **Site 2**. This distribution of preferred activities is based on the observation that the kinetics of MMAc formation over ZEO-1 are nearly identical to those reported for FAU, which has one type of large cavity. By contrast, the kinetics of MF formation observed for ZEO-1 more nearly resemble those seen for MFI, which has small cavities. Figs. 10(a) and 10(c) show that IR peak at 1733 $cm^{-1}$ for MFZ is highly suppressed when CO is present, indicating that DMM disproportionation is inhibited. More direct evidence for the kinetics of DMM disproportionation over **Site 2**, was obtained by carrying out the reaction over BEA, which only contains 12×12-MRs channel intersections. As see in Fig. S14, BEA exhibits high disproportionation activity in the absence of CO, but the rates of MF formation decrease significantly upon the addition of CO to the feed. Accordingly, the DMM carbonylation and disproportionation mechanisms for ZEO-1 are proposed to occur on two types of sites.

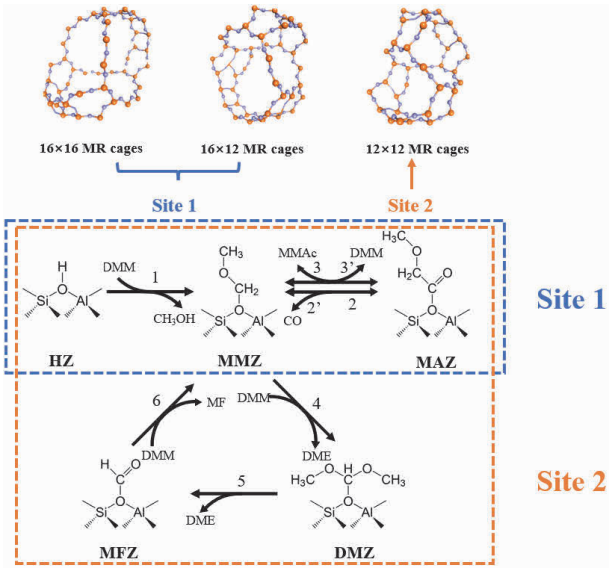


**Fig. 13.** Proposed mechanism for DMM carbonylation and disproportionation over different active sites in ZEO-1 [2,14]. The blue dashed square demonstrates the reaction cycle over DMM carbonylation active site (**Site 1**), and the orange dashed square demonstrates the reaction cycle over DMM disproportionation active site (**Site 2**).

DMM conversion initiates from its interaction with Brönsted acid sites to generate MMZ intermediate and methanol for both **Site 1** and **Site 2** and this process can be considered as the induction period for both processes. Then, CO insertion to MMZ transfer the surface MMZ to MAZ species and generate the new C-C bond preferably over **Site 1**. A competitive route to this step is the attack of DMM to MMZ to form the surface MFZ species over **Site 2**. These acyl intermediates, MAZ and MFZ, can then be attacked by DMM to generate MMAc and MF, respectively, via methoxylation, and thereby regenerating the MMZ precursor over **Site 1** or **Site 2**. Therefore, it is proposed that the active centers could be occupied by MMZ, MAZ and MFZ species in agreement with evidence from IR spectroscopy. The relative concentrations of these intermediates depend on competitive rates of their generation and consumption, which, in turn, influences the overall product selectivity.

Based on this mechanistic understanding, the kinetics of DMM carbonylation and disproportionation on ZEO-1 can be interpreted in terms of the following steps:

$$HZ + DMM \xrightarrow{k_1} MMZ + CH_3OH \quad (R7)$$

$$MMZ + CO \underset{k'_2}{\overset{k_2}{\leftrightarrow}} MAZ \quad (R8)$$

$$MAZ + DMM \underset{k'_3}{\overset{k_3}{\leftrightarrow}} MMZ + MMAc \quad (R9)$$

$$MMZ + DMM \xrightarrow{k_4} DMZ + DME \quad (R10)$$

$$DMZ \xrightarrow{k_5} DME + MFZ \quad (R11)$$

$$MFZ + DMM \xrightarrow{k_6} MMZ + MF \quad (R12)$$

The rates of MMAc and MF formation can be expressed by Eqs. (5) and (6) [1,2]. These equations were derived based on the assumption that the adsorption and desorption of MMZ, DMZ, MFZ and MAZ are quasi-equilibrated. $k_x$ and $k'_x$ are the forward and reverse reaction rate constants for each elementary step, $x$ = 1 to 6 for $k_x$ and 2 to 3 for $k'_x$. $P_a$ is the partial pressure of corresponding reactant or products, a could be DMM, DME, MF and MMAc. $\theta_b$ is the surface coverage of DMM carbonylation and disproportionation intermediates, b could be MMZ, DMZ, MFZ and MAZ. Reaction 7, DMM decomposition to MMZ at Brönsted acid sites, is rapid and can be neglected. Therefore, the expressions for MMAc and MF formation shown below are derived from reaction R8 to R12. The derivation of these rate expressions is given in the SI.

$$r_{MMAc} = \frac{\frac{k_2 k_3 P_{CO} P_{DMM} - k'_2 k'_3 P_{MMAc}}{k'_2 + k_3 P_{DMM}}}{1 + \frac{k_2 P_{CO} + k'_3 P_{MMAc}}{k'_2 + k_3 P_{DMM}} + \frac{k_4}{k_5} P_{DMM} + \frac{k_4}{k_6}} \quad (5)$$

$$r_{MF} = \frac{k_4 P_{DMM}}{1 + \frac{k_2 P_{CO} + k'_3 P_{MMAc}}{k'_2 + k_3 P_{DMM}} + \frac{k_4}{k_5} P_{DMM} + \frac{k_4}{k_6}} \quad (6)$$

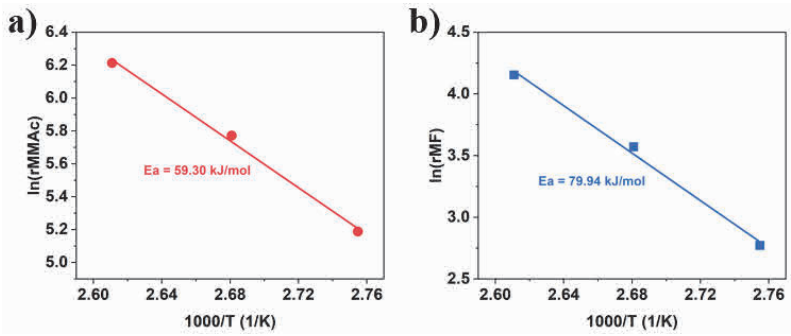


**Fig. 14.** DMM carbonylation and disproportionation apparent activation energy of ZEO-1 exposed to DMM/CO. Reaction conditions: 0.008 g ZEO-1, 363–383 K, $P_{DMM}$ = 43 kPa, GHSV = 750 L $g_{cat}^{-1}$ $h^{-1}$ at 2 MPa.

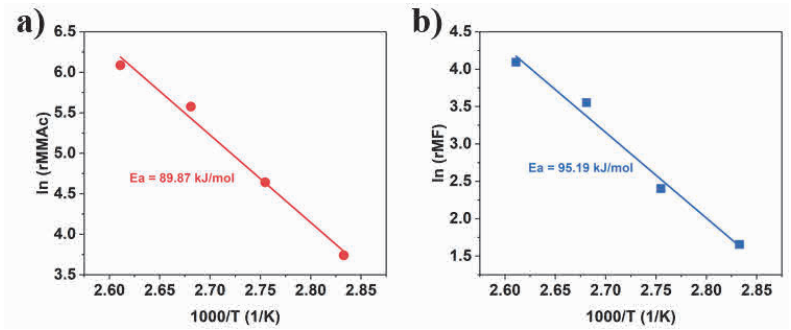


**Fig. 15.** DMM carbonylation and disproportionation apparent activation energy of FAU (Si/Al = 30) exposed to DMM/CO. Reaction conditions: 0.01 g FAU, 353–383 K, $P_{DMM}$ = 43 kPa, GHSV = 300-1200 L $g_{cat}^{-1}$ $h^{-1}$ at 2 MPa.

At low DMM conversion, the decomposition rate of MMAc is much slower than the methoxylation of MAZ, suggesting that the values of $k'_3$ is small and can be ignored. The expressions for the rates of MMAc and MF formation can then be simplified to Eqs. (7) and (8) givens below. The denominators of the expressions for $r_{MMAc}$ and $r_{MF}$ are identical. The term $k_2P_{CO}/(k'_2 + k_3P_{DMM})$represents site occupancy by surface MAZ, while term $k_4P_{DMM}/k_6$ and $k_4/k_6$ represents site occupancy by disproportionation intermediates, DMZ and MFZ.

$$r_{MMAc} = \frac{\frac{k_2k_3P_{CO}P_{DMM}}{k_2 + k_3P_{DMM}}}{1 + \frac{k_2P_{CO}}{k_2 + k_3P_{DMM}} + \frac{k_4}{k_5}P_{DMM} + \frac{k_4}{k_6}} \quad (7)$$

$$r_{MF} = \frac{k_4P_{DMM}}{1 + \frac{k_2P_{CO}}{k_2 + k_3P_{DMM}} + \frac{k_4}{k_5}P_{DMM} + \frac{k_4}{k_6}} \quad (8)$$

Comparison of the rates of DMM carbonylation for FAU and ZEO-1 under differential reaction conditions shows that ZEO-1 exhibits a high TOF activity that is similar to that for FAU prepared with Si/Al = 30, for which the spatial separation between Al is large. The rate expression for carbonylation (Eq. (7)) can be further simplified on the assumption that the rate coefficients determined for FAU are not very different from those for ZEO-1 over **Site 1** [2]. If this is the case, the second and third terms in the denominators of Eq. (7) are small, and these expressions are further simplified to:

$$r_{MMAc} = \frac{\frac{k_2k_3P_{CO}P_{DMM}}{k_2 + k_3P_{DMM}}}{1 + \frac{k_4}{k_5}P_{DMM}} \quad (9)$$

The rate expressions for DMM carbonylation given by Eq. (9) can be used to interpret the rate data presented in Fig. 5. As shown under conditions of low DMM conversion, the rate of MMAc formation exhibits a linear dependence on CO partial pressure and a weak inverse dependence on the partial pressure of DMM, which is what would be predicted by Eq. (9), and has been observed for FAU [2]. However, the MF formation rate displays a strong negative dependence on CO partial pressure (Fig. 5(b)), like that observed for BEA (Fig. S14). As discussed above, the similarity in the sensitivity of the rare MF formation over ZEO-1 and BEA should be attributed to the formation of this product in the 12×12-MRs intersections of both zeolites (**Site 2** in ZEO-1). The inhibitory effect of CO on DMM disproportionation over such sites is ascribed to the slow rate of MAZ methoxylation with DMM on **Site 2**, resulting in a decrease in the fraction of **Site 2** occupied by DMZ and MFZ, the precursors to DMM disproportionation, which occurs *via* reaction of DMM with MMZ (Fig. 13). Inhibition of MF formation by CO for ZEO-1 suggests that the value of the second term in the denominator of Eq. (8) is significant because of a lower value of $k_3$ for **Site 2**. It then follows that the rate of MF formation will decrease with increasing CO partial pressure, all other variables being the same.

Formation rates of MMAc and MF evaluated at different reaction temperatures shown in Figs. 14 and 15 were used to determine the apparent activation barriers for the DMM carbonylation and disproportionation. Fig. 14 shows that the apparent activation energies for DMM carbonylation and disproportionation are 59.30 and 79.94 kJ $mol^{-1}$, respectively, for ZEO-1, whereas those for DMM carbonylation and disproportionation catalyzed by FAU (Si/Al = 30), the apparent activation energies are 88.97 and 95.19 kJ $mol^{-1}$, respectively (Fig. 15).

Larger difference of DMM disproportionation and carbonylation apparent activation energy of ZEO-1 means that the selectivity of ZEO-1 for MMAc formation decreases by a larger degree relative to MF/DME formation with increased reaction temperature.

This facile process for DMM carbonylation also shows obvious contrast with the carbonylation of surface methyl group during the DME carbonylation, which exhibits a much higher activation energy of 100–140 kJ mol$^{-1}$ [33,36,37]. While both processes are similar for CO insertion to generate acyl intermediate through a carbocation-mediated mechanism, the activation energy for carbonylation of methyl carbocations involved in the carbonylation of DME is higher because methyl carbocation is less favorably stabilized than the methoxymethyl carbocation involved in DMM carbonylation [4]. The DME carbonylation could, therefore, only be efficiently catalyzed within zeolites containing 8-MRs channels like MOR, FER, which could impose a strong "confinement effect" for the formation of acyl species. Due to the much higher reactivity of MMZ species, the promotion effect of zeolite the "confinement effect" on the nucleophilic attack of CO to MMZ to generate MAZ is quite limited. Actually, too tight a fit between zeolite reaction spaces with DMM molecule will seriously inhibit the carbonylation process by reducing the rate of MAZ methoxylation.

On the other hand, based on the kinetic understanding, the optimal reaction conditions for MMAc formation are low temperature (< 393 K) to avoid the decomposition of the MAZ intermediate and high pressure (> 1 MPa) to reduce the influence of disproportionation. However, under such conditions, the diffusion of the reactant as well as the product would be hindered, which might reduce the catalytic activity and stability because of the diffusion limitation, especially for reactants with large size. Therefore, we conclude that a zeolite with large pores, large reaction spaces, and a more spatially distributed framework Al species promotes DMM carbonylation activity, selectivity, and stability. With the rapid development of zeolitic materials in recent years, more advanced zeolite materials with further improved DMM carbonylation performance could be developed, contributing to the production of MEG and GA from syngas through a non-metal-based route.

## 4. Conclusions

This study investigates the catalytic performance of ZEO-1 zeolite for both DMM carbonylation to form MMAc and DMM disproportionation to form MF and DME, and compares the activity, selectivity, and stability of this zeolite to those of FAU. The rate of MMAc formation normalized by accessible Brönsted acid sites is 2.5 times higher for ZEO-1 (Si/Al = 21) relative to FAU (Si/Al = 15), indicating the superior catalytic activity of ZEO-1 to FAU with slightly higher Al density. Furthermore, due to the enhancement caused by spatial separation of active sites, a comparable high DMM carbonylation TOF activity is observed for FAU with a high Si/Al ratio of 30, comparable to that of ZEO-1. This observation suggests the remarkable advantage of large-void zeolite, e.g., ZEO-type zeolites, for carbonylation of large reactants. *In-situ* IR spectroscopy also shows that the concentration of MAZ, a critical intermediate for DMM carbonylation, characterized by an IR band at 1744 cm$^{-1}$ is comparable for ZEO-1 than FAU, but the diffusion of the MMAc product is faster in ZEO-1.

The kinetics of MMAc formation over ZEO-1 and FAU exhibit a similar dependence on CO partial pressures, while that for MF and DME formation from DMM disproportionation are quite different. ZEO-1 and FAU exhibit a first-order dependence of the rate of MMAc formation on CO partial pressure. The apparent activation energy for MMAc formation on ZEO-1 is 59.30 kJ/mol, lower than that for FAU, 89.87 kJ mol$^{-1}$. For DMM disproportionation, ZEO-1 exhibits a strongly inverse dependence of the rate of MF formation with increasing CO partial pressure. In contrast, rate of MF formation on FAU is almost independent of CO partial pressure. For both zeolites, the dependence of the rate of MF formation on DMM partial pressure is slightly positive. Another notable difference is the disproportionation apparent activation energy, which for ZEO-1 is 79.94 kJ mol$^{-1}$ and for FAU is 95.19 kJ mol$^{-1}$.

The similarities in the kinetics of MMAc formation on ZEO-1 and FAU, and the differences in the kinetics of MF/DME formation on the two zeolites are attributed to differences in the pore structure of these materials. ZEO-1 contains three types of cages made up of 16×16-MRs, 16×12-MRs, and 12×12-MRs, whereas the supercage in FAU are made up of 12×12-MRs. It is proposed that ZEO-1 contains two dominant types of sites specifically for DMM carbonylation and disproportionation. **Site 1** is located in large cages formed by 16×16-MRs and 16×12-MRs, whereas **Site 2** is located in small cages formed by 12×12-MRs. It is proposed that **Site 1** is active predominantly for MMAc formation and that **Site 2** is active predominantly for MF/DME formation. The proposed distribution of site activities is supported by the observation of inhibition of MF formation by CO on BEA, which has cages composed exclusively of 12×12-MRs.

This work provides important insights into the zeolite properties required for the efficient production of MMAc, a product that can be used to produce MEG and GA, and also directs a promising application for large-void structured zeolite materials. Based on the current understanding, a zeolite material with large pores, large reaction spaces and more spatially distributed framework Al species could promote both the DMM carbonylation activity, selectivity, and stability by promoting the MAZ formation, transformation, and guest molecules diffusion.

## Note

The authors declare no competing financial interest.

## Acknowledgments

This work was supported by the National Natural Science Foundation of China (22472173). LQ acknowledges the Youth Innovation Promotion Association, the Chinese Academy of Sciences (2023193), ATB acknowledges support by the Office of Science, Office of Basic Energy Sciences, of the U.S. Department of Energy (DOE) under Contract DE-AC02-05CH11231.

The ZeoMat Group acknowledges the starting grant provided by QIBEBT and the support provided by the Shandong Energy Institute (SEI S202107). V.V. acknowledges the collaboration in the Sino-French International Research Network "Zeolites" framework. P.L. acknowledges the support by QIBEBT International Collaboration Project (202305). We gratefully thank the meaningful discussion with Dr. Shiping Liu, Prof. Peng Tian.

## Electronic supporting information

Supporting information is available in the online version of this article.

## References

[1] F. E. Celik, T.-J. Kim, A. T. Bell, *J. Catal.*, **2010**, 270, 185–195.
[2] F. E. Celik, T. Kim, A. N. Mlinar, A. T. Bell, *J. Catal.*, **2010**, 274, 150–162.
[3] F. E. Celik, T. J. Kim, A. T. Bell, *Angew. Chem. Int. Ed.*, **2009**, 48, 4813–4815.
[4] J. Yao, Y. Wang, S. S. Bello, G. Xu, L. Shi, *Appl. Organomet. Chem.*, **2020**, 34, e5925.
[5] D. Zhang, L. Shi, Y. Wang, F. Chen, J. Yao, X. Li, Y. Ni, W. Zhu, Z. Liu, *Catal. Today*, **2018**, 316, 114–121.
[6] Z. Xie, C. Chen, B. Hou, D. Sun, H. Guo, J. Wang, D. Li, L. Jia, *J. Phys. Chem. C*, **2018**, 122, 9909–9917.
[7] V. Shapovalov, A. T. Bell, *J. Phys. Chem. C*, **2010**, 114, 17753–17760.
[8] W. Dai, C. Wang, B. Tang, G. Wu, N. Guan, Z. Xie, M. Hunger, L. Li, *ACS Catal.*, **2016**, 6, 2955–2964.
[9] C. Wang, N. Xu, K. Huang, B. Liu, P. Zhang, G. Yang, H. Guo, P. Bai, S. Mintova, *Chem. Eng. J.*, **2023**, 466, 143136.
[10] F. E. Celik, H. Lawrence, A. T. Bell, *J. Mol. Catal. A*, **2008**, 288, 87–96.
[11] L. Rong, Z. Xu, J. Sun, G. Guo, *J. Energy Chem.*, **2018**, 27, 238–242.
[12] W. Reutemann, H. Kieczka, *Ullmann's Encyclopediaof Industrial Chemistry*, **2011**, 16, 67–82.
[13] http://www.dicp.cas.cn/xwdt/kyjz/202212/t20221202_6565978.html.
[14] Q. F. Lin, Z. R. Gao, C. Lin, S. Y. Zhang, J. F. Chen, Z. Q. Li, X. L. Liu, W. Fan, J. Li, X. B. Chen, M. A. Camblor, F. J. Chen, *Science*, **2021**, 374, 1605–1608.
[15] J. Li, Z. R. Gao, Q. F. Lin, C. X. Liu, F. X. Gao, C. Lin, S. Y. Zhang, H. Deng, A. Mayoral, W. Fan, S. Luo, X. B. Chen, H. He, M. A. Camblor, F. J. Chen, J. H. Yu, *Science*, **2023**, 379, 283–287.
[16] Z. R. Gao, H. J. Yu, F. J. Chen, A. Mayoral, Z. J. Niu, Z. W. Niu, X. T. Li, H. Deng, C. Márquez-Alvarez, H. He, S. T. Xu, Y. D. Zhou, J. Xu, H. Xu, W. Fan, S. R. G. Balestra, C. Ma, J. Z. Hao, J. Li, P. Wu, J. H. Yu, M. A. Camblor, *Nature*, **2024**, 628, 99–103.
[17] T. Clingenpeel, A. Biaglow, *J. Am. Chem. Soc.*, **1997**, 119, 5077–5078.
[18] G. T. Kokotailo, S. L. Lawton, D. H. Olson, D. H. Olson, W. M. Meier, *Nature*, **1978**, 272, 437–438.
[19] P. Morales-Pacheco, F. Alvarez, L. Bucio, J. M. Domínguez, *J. Phys. Chem. C*, **2009**, 113, 2247–2255.
[20] J. M. Newsam, M. M. J. Treacy, W. T. Koetsier, C. B. Degruyter, *Proc. Royal Soc. A*, **1988**, 420, 375–405.
[21] A. Inayat, I. Knoke, E. Spiecker, W. Schwieger, *Angew. Chem. Int. Ed.*, **2012**, 51, 1962–1965.
[22] M. A. Camblor, A. Corma, S. Valencia, *Microporous Mesoporous Mater.*, **1998**, 25, 59–74.
[23] X. Wang, Y. K. Lv, S. H. Zhu, X. F. Wang, C. B. Deng, *Catalysts,* **2021**, 11, 962.
[24] Y. Q. Chen, W. X. Wu, N. W. Liu, L. Shi, X. Meng, *New J. Chem.*, **2023**, 47, 18018–18026.
[25] M. Liu, Y. X. Yin, X. W. Guo, C. S. Song, *Ind. Eng. Chem. Res.*, **2017**, 56, 8850–8856.

## Graphical Abstract

*Chin. J. Catal.*, 2025, 68: 230–245 doi: 10.1016/S1872-2067(24)60187-7

**Dimethoxymethane carbonylation and disproportionation over extra-large pore zeolite ZEO-1: Reaction network and mechanism**

Shaolei Gao, Peng Lu, Liang Qi *, Yingli Wang, Hua Li, Mao Ye, Valentin Valtchev, Alexis T. Bell, Zhongmin Liu *
*Dalian Institute of Chemical Physics, Chinese Academy of Sciences, China; University of Chinese Academy of Sciences, China; Qingdao Institute of Bioenergy and Bioprocess Technology, China; Université de Caen Normandie, France; Centre national de la Recherche Scientifique, France; Lawrence Berkeley National Laboratory, USA; University of California, USA*

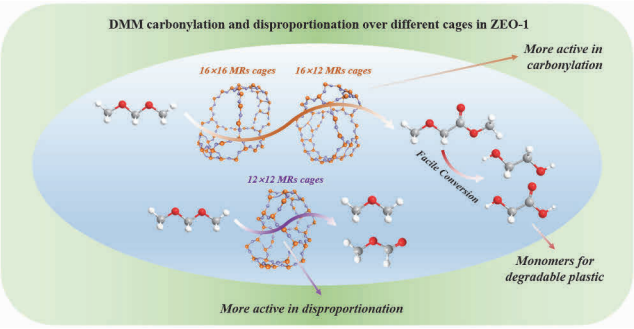


Dimethoxymethane (DMM) carbonylation provide a mild, green and sustainable route for production of degradable plastic monomers, glycolic Acid (GA). ZEO-1 zeolite containing extra-large reaction space exhibits high DMM carbonylation activity, selectivity and excellent stability.

[26] M. Fahda, J. Fayek, E. Dib, H. Cruchade, N. Pichot, N. Chaouati, L. Pinard, P. S. Petkov, G. N. Vayssilov, A. Mayoral, B. Witulski, L. Lakiss, V. Valtchev, *Chem. Mater.*, **2024**, 36, 5405–5421.
[27] C. J. Baranowski, T. Fovanna, M. Roger, M. Signorile, J. McCaig, A. M. Bahmanpour, D. Ferri, O. Kröcher, *ACS Catal.*, **2020**, 10, 8106–8119.
[28] J. B. Wu, Z. P. Sun, Z. H. Wei, Z. F. Qin, Y. X. Zhao, *Catal. Lett.*, **2021**, 151, 670–684.
[29] H. Susi, T. Zell, *Spectrochim. Acta*, **1963**, 19, 1933–1945.
[30] G. J. Millar, C. H. Rochester, K. C. Waugh, *J. Chem. Soc. Faraday Trans.*, **1991**, 87, 2785–2793.
[31] L. Qi, S. Das, Y. Zhang, D. Nozik, B. C. Gates, A. T. Bell, *J. Am. Chem. Soc.*, **2023**, 145, 2911–2929.
[32] M. Boronat, C. Martínez, A. Corma, *Phys. Chem. Chem. Phys.*, **2011**, 13, 2603–2612.
[33] M. Boronat, C. Martínez-Sánchez, D. Law, A. Corma, *J. Am. Chem. Soc.*, **2008**, 130, 16316–16323.
[34] M. Koehle, Z. Zhang, K. A. Goulas, S. Caratzoulas, D. G. Vlachos, R. F. Lobo, *Appl. Catal. A*, **2018**, *564*, 90–101.
[35] T.-H. Chen, D. G. Vlachos, S. Caratzoulas, *ACS Catal.*, **2021**, 11, 9916–9925.
[36] Z. Xiong, G. Qi, E. Zhan, Y. Chu, J. Xu, J. Wei, N. Ta, A. Hao, Y. Zhou, F. Deng, *Chem*, **2023**, 9, 76–92.
[37] W. Chen, G. Li, X. Yi, S. J. Day, K. A. Tarach, Z. Liu, S.-B. Liu, S. C. Edman Tsang, K. Góra-Marek, A. Zheng, *J. Am. Chem. Soc.*, **2021**, 143, 15440–15452.

# 超大孔分子筛ZEO-1催化甲缩醛羰基化及歧化反应: 反应网络与机理研究

高绍磊[a,b], 卢　鹏[c], 亓　良[a,*], 王莹利[a], 李　华[a], 叶　茂[a], Valentin Valtchev [d], Alexis T. Bell [e,f], 刘中民[a,b,*]

[a]中国科学院大连化学物理研究所, 洁净能源国家实验室, 低碳催化技术国家工程研究中心, 辽宁大连116023, 中国
[b]中国科学院大学, 中国科学院, 北京100049, 中国
[c]青岛生物能源与过程研究所, 分子筛材料研究组, 山东青岛266101, 中国
[d]卡昂大学,法国国立卡昂高等工程师学院, 法国国家科学研究中心, 催化与光谱化学实验室, 卡昂, 法国
[e]劳伦斯伯克利国家实验室, 加利福尼亚州伯克利, 美国
[f]加利福尼亚大学伯克利分校, 化学与生物分子工程系, 加利福尼亚州伯克利, 美国

**摘要**: 甲缩醛羰基化反应产物甲氧基乙酸甲酯是生产乙醇酸、乙醇酸甲酯及乙二醇的前驱体. 乙二醇可作为化工原料, 也可直接应用于防冻剂和溶剂. 而乙醇酸或乙醇酸甲酯的聚合产物聚乙醇酸是生产可生物降解塑料的原料, 符合绿色化学和环境保护的发展要求, 应用前景广阔. 以甲缩醛羰基化为核心的乙醇酸、乙醇酸甲酯和乙二醇生产路径具有条件温和、效率较高和易于工业放大等优点. 当前研究仍局限于FAU是催化甲缩醛羰基化的最佳分子筛催化剂. 对具有高活性、高选择性和高稳定性的新型分子筛催化剂探索未见报道, 也是当前研究的重点和难点.

本文选择了近期在Science杂志新报道(*Science*, **2021**, 374, 1605–1608)的含16元环的超大孔分子筛ZEO-1, 合成并将其用于甲缩醛羰基化反应. 首先与文献报道具有最佳单位点活性的FAU分子筛进行甲缩醛羰基化对比, 明确了ZEO-1分子筛催化甲缩醛羰基化高活性、高选择性和高稳定性的特征. 随后利用原位红外光谱观察了ZEO-1分子筛催化甲缩醛羰基化及其歧化副反应中间体甲氧基亚甲基、甲氧基乙酰基和甲酰基的动态演变过程, 并尝试将中间体表面生成量与反应活性和分子筛扩散性能相关联. 随后在近动力学条件下研究了一氧化碳和甲缩醛分压对甲缩醛羰基化及歧化活性的影响, 发现羰基化活性与一氧化碳分压呈线性相关而与甲缩醛分压呈负相关, 歧化活性与一氧化碳分压呈负相关而与甲缩醛分压呈正相关, 表明ZEO-1催化甲缩醛羰基化过程中歧化反应竞争的影响不可忽略. ZEO-1分子筛中活性位点同时分布于16×16元环, 16×12元环和12×12元环交叉位形成的笼中, 不同位点因所处反应空间尺寸的不同而具有明显不同的甲缩醛羰基化及歧化倾向性. 基于甲缩醛羰基化及歧化反应, 红外和动力学实验结果提出了ZEO-1不同位点催化甲缩醛羰基化及歧化的反应循环机理. 将16×16元环和16×12元环交叉位组成的尺寸较大的笼中的Brönsted酸中心定义为羰基化活性中心. 12×12元环交叉位组成的尺寸较小的笼中的Brönsted酸中心为歧化活性中心. 最后, 推导了甲缩醛羰基化及歧化动力学方程且提出的动力学方程结果与动力学实验规律相一致.

综上, 本工作探索了具有超大反应空间的ZEO-1分子筛催化甲缩醛羰基化反应, 明确了ZEO-1分子筛催化甲缩醛羰基化的高活性、高选择性和高稳定性. 分析了ZEO-1分子筛催化甲缩醛羰基化及歧化反应机理与动力学特征, 为甲缩醛羰基化分子筛催化剂的筛选改进提供了初步理论指导.

**关键词**: 甲缩醛羰基化; 甲缩醛歧化; 分子筛; 原位红外光谱; 动力学; 反应机理

收稿日期: 2024-10-23. 接受日期: 2024-11-25. 上网时间: 2025-01-10.
*通讯联系人. 电子信箱: qlyanfei920@dicp.ac.cn (亓良), zml@dicp.ac.cn (刘中民).
基金来源: 国家自然科学基金(22472173); 中国科学院青年创新促进会(2023193); 山东能源研究院(SEI S202107); 中国科学院青岛生物能源与过程研究所国际合作项目(202305).